

DMRG Calculations of the Low-lying Excitations and Nonlinear Optical

Properties of poly(*para*-phenylene)

William Barford¹, Robert J. Bursill² and Mikhail Yu. Lavrentiev^{3*}

^{1,3}Department of Physics, The University of Sheffield, Sheffield, S3 7RH, UK

²School of Physics, University of New South Wales, Sydney, NSW 2052, Australia

Email: ¹W.Barford@sheffield.ac.uk, ²ph1rb@newt.phys.unsw.edu.au, ³M.Lavrentiev@sheffield.ac.uk

Abstract

A phenomenological two molecular orbital (2-MO) model of poly(*para*-phenylene) (PPP) is introduced. Its parameters are determined by fitting its predictions to exact Pariser-Parr-Pople model calculations of benzene and biphenyl, and it is solved using the density matrix renormalisation group method. It is shown that there exists a band of $^1B_u^-$ excitons below the band states. In the long chain limit the lowest exciton is situated 3.3 eV above the ground state, consistent with experimental data. The calculated particle-hole separation of these excitons indicates that they are tightly bound, extending over only a few repeat units. The lowest band state is found to be a covalent $2^1A_g^+$ state, whose energy almost coincides with the charge gap E_G . Lying just above the $2^1A_g^+$ state is a band $^1B_u^-$ state (the $n^1B_u^-$ state). The particle-hole separation of the band states scales linearly with oligomer size. The binding energy of the $1^1B_u^-$ exciton is determined rigorously as 0.74 eV.

The dipole matrix elements and oscillator strengths for the transitions between the lowest $^1A_g^+$ and $^1B_u^-$ states are calculated and the NLO properties of PPP, such as electroabsorption (EA) and third harmonic generation, are investigated. A comparison of the EA spectrum with the experimental data show that the main features of the experimental spectrum are well described in the 2-MO Hamiltonian.

Only five states account for most of the calculated EA. These are the $1^1A_g^+$, $1^1B_u^-$, $2^1A_g^+$, $n^1B_u^-$ and another band $^1A_g^+$ state, the $k^1A_g^+$, thus confirming the essential states model. An analysis of the particle excitation weight of these states indicates that they are predominately single particle in character.

PACS numbers: 42.70Jk, 71.20Rv, 78.66Qn, 71.35Cc

1 Introduction

Since the first light-emitting device based on poly(*para*-phenylenevinylene) (PPV) was reported [1], the non-linear optical (NLO) properties of conjugated polymers have been extensively investigated. Amongst the numerous systems studied, poly(*para*-phenylene) (PPP), being a linear chain of phenyl rings, possesses one of the simplest structures. However, its electronic structure and the nature of the blue light emission [2] are still controversial. First-principles local-density approximation studies by Ambrosch-Draxl *et al.* [3] suggest that the optical properties of PPP can be explained by a purely band picture, with intragap non-linear excitations suppressed by three-dimensional effects. However, recent experimental results on the electroabsorption (EA) and photoinduced absorption (PA) in substituted PPP by Lane *et al.* [4] are explained by the presence of non-linear excitations, such as singlet and triplet excitons, and charged polarons.

The aim of this paper is to clarify the rôle and importance of the non-linear excitations in PPP by calculating its electronic structure and NLO properties in a realistic Hamiltonian. The EA spectrum compares favourably with recent experiments. We identify the key states which participate in the NLO processes. Moreover, by calculating the particle-hole separation of these states, we identify the band gap as the threshold state whose particle-hole separation increases linearly with oligomer size. This enables a rigorous determination of the band gap to be made.

In a recent paper [5] the four molecular orbital (4-MO) model and the two molecular orbital (2-MO) model of PPP were introduced. These models are derived from the Pariser-Parr-Pople model of π conjugated systems. The 4-MO model gives a qualitative description of the long and short axis polarised excitations, while the 2-MO model provides a description of just the long axis polarised excitations. However, using the parameters obtained directly from the Pariser-Parr-Pople model it is not possible to obtain quantitative agreement between the predictions of the 2-MO model and experiment. This failure of the 2-MO model is a consequence of neglecting important many body correlations between the active and frozen phenyl molecular orbitals. In this paper, therefore, we present a phenomenological 2-MO model whose parameters are chosen to fit exact Pariser-Parr-Pople

model calculations on benzene and biphenyl. This phenomenological model will be introduced and discussed at some length in this paper.

As well as our earlier work [6], there have been a number of theoretical calculations on PPP. Brédas has used the VEH pseudopotential technique [7], Champagne et al. have performed Hartree-Fock calculations [8], and Ambrosch-Draxl et al. have performed density functional calculations using LAPW and pseudopotentials [3]. Rice et al. [9] have developed a phenomenological, microscopic model based on the molecular excitations of benzene. The absorption bands are calculated using an approximate Kubo formalism.

The structure of a PPP chain is shown schematically in Fig. 1. The electronic states can be classified according to their spatial, spin and particle-hole symmetries. In this paper we only consider states which are symmetric under reflection in the $x-z$ plane, and either symmetric or anti-symmetric under reflection in the $x-y$ plane. This will correspond to the low energy excitations. The ground state belongs to the $^1A_g^+$ (spin singlet, space- and particle-hole-symmetric) symmetry sector. One-photon excitations occur between the $^1A_g^+$ and the $^1B_u^-$ (spin singlet, odd space and particle-hole symmetry) symmetry sectors.

Non-linear processes in polymers with inversion symmetry are determined by the third-order susceptibility $\chi^{(3)}(-\omega_1 - \omega_2 - \omega_3; \omega_1, \omega_2, \omega_3)$, which can be calculated as a sum over intermediate states (see, e.g., [10]). It was suggested several years ago that most of the NLO properties can be described by an “essential states” model [11, 12, 13, 14]. The concept of the essential states model implies that there is a restricted set of states responsible for most of the NLO properties of the system. Usually, these are the ground state ($^1A_g^+$), the lowest excited (excitonic) $^1B_u^-$ state, the $m^1A_g^+$ state, which is the $^1A_g^+$ state most strongly related to the $^1B_u^-$ states through one-photon excitations, and the band threshold $n^1B_u^-$ state. We investigate the validity of this approach for PPP.

Until recently, numerical investigations of one-dimensional systems with strong electron-electron interactions were limited to exact diagonalisations of short chains, to approximate single configuration

interaction calculations or to the use of density functional theory. A key aspect of this work is that we perform essentially exact calculations on our model using the density matrix renormalisation group (DMRG) method. We check the numerics by comparing DMRG results with exact results in the non-interacting limit, by comparing DMRG and exact diagonalisation calculations for a 7 unit oligomer and by monitoring the convergence of results with the parameter m (which controls the amount of Hilbert space truncation and hence the DMRG error) for longer systems in the interacting case.

The plan of this paper is as follows. In the next section the phenomenological model will be introduced and parameterised. In §3 the energy and root-mean-square size of the low-lying states are calculated as a function of oligomer size, thus identifying the band threshold. The single particle excitation weight of the wavefunctions is also investigated. In §4 the dipole moments between states are calculated, thus identifying the key states in the NLO processes. The linear susceptibility is also calculated. In §5 we turn to the calculation of the EA and THG spectra using the sum-over-states method. Finally, we conclude in §6.

2 The Phenomenological Model and Hamiltonian

The starting point for the molecular orbital approach used in this paper is the well-known Pariser-Parr-Pople or extended Hubbard Hamiltonian:

$$H = - \sum_{\langle ij \rangle \sigma} t_{ij} \left[c_{i\sigma}^\dagger c_{j\sigma} + \text{h.c.} \right] + U \sum_i \left(n_{i\uparrow} - \frac{1}{2} \right) \left(n_{i\downarrow} - \frac{1}{2} \right) + \frac{1}{2} \sum_{i \neq j} V_{ij} (n_i - 1)(n_j - 1), \quad (1)$$

Here, $c_{i\sigma}^\dagger$ and $c_{i\sigma}$ are creation and destruction operators, respectively, for a π electron with spin σ on carbon site i , $n_{i\sigma} = c_{i\sigma}^\dagger c_{i\sigma}$ is the number operator, $n_i = n_{i\uparrow} + n_{i\downarrow}$ and t_{ij} is the transfer integral. U and V_{ij} are Coulomb repulsion parameters for electrons occupying one site and sites i and j , respectively.

We use the Ohno parameterisation for the Coulomb interaction,

$$V_{ij} = \frac{U}{(1 + \alpha r_{ij}^2)^{1/2}}, \quad (2)$$

where $\alpha = (U/14.4)^2$, thus ensuring that $V_{ij} \rightarrow e^2/(4\pi\epsilon_0 r_{ij})$ as $r_{ij} \rightarrow \infty$, and r_{ij} is the inter-atomic distance in Å. The optimal parameterisation for PPP, which was derived in [15], is $U = 10.06$ eV, the phenyl bond transfer integral, $t_p = 2.539$ eV and the single bond transfer integral, $t_s = 2.22$ eV.

2.1 The Model

The six atomic π -orbitals of a phenyl ring $c_{i\sigma}^\dagger, i = 1, \dots, 6$ may be transformed to six molecular orbitals (MOs), $a_{\alpha\sigma}^\dagger$. This approach for phenyl based semiconductors was used earlier by Soos *et al.* [16]. Recently, Chandross *et al.* [17] employed a similar approach in their work on the characterization of excited states in conjugated polymers. It was suggested in [6] that the low lying excitations could be described by only two of the resulting MOs, namely, one of the two degenerate e_{1g} HOMO states and one of the two degenerate e_{2u} LUMO states. This is the so-called 2-MO model. The other HOMO and LUMO states are non-bonding, because the wave function amplitude on the bridging carbon atoms is zero. The (occupied) a_{2u} and (empty) b_{2g} states are situated far away in energy from the HOMO and LUMO, and are assumed to play only a minor role in the low-energy excitations. Below, the HOMO orbital is denoted by $|1\rangle$ and the LUMO orbital is denoted by $|2\rangle$.

With two MOs left, and neglecting the three and four centre two-electron integrals and Coulomb interactions beyond nearest neighbour phenylene units, the transformation from the atomic to the molecular orbital basis results in the following Hamiltonian:

$$\begin{aligned}
H = & - \sum_{i\alpha\beta\sigma} t_{\alpha\beta} \left[a_{i\alpha\sigma}^\dagger a_{i+1\beta\sigma} + \text{h.c.} \right] + \sum_{i\alpha} \epsilon_\alpha (n_{i\alpha} - 1) + U \sum_{i\alpha} \left(n_{i\alpha\uparrow} - \frac{1}{2} \right) \left(n_{i\alpha\downarrow} - \frac{1}{2} \right) \\
& + \frac{U}{2} \sum_{i\alpha\neq\beta} (n_{i\alpha} - 1)(n_{i\beta} - 1) + V \sum_{i\alpha\beta} (n_{i\alpha} - 1)(n_{i+1\beta} - 1) \\
& - X \sum_{i\alpha\neq\beta} \left[\mathbf{S}_{i\alpha} \cdot \mathbf{S}_{i\beta} + \frac{1}{4} (n_{i\alpha} - 1)(n_{i\beta} - 1) \right] \\
& + \frac{P}{2} \sum_{i\alpha\neq\beta\sigma} a_{i\alpha\sigma}^\dagger a_{i\alpha\bar{\sigma}}^\dagger a_{i\beta\bar{\sigma}} a_{i\beta\sigma}, \quad (3)
\end{aligned}$$

where $\mathbf{S}_{i\alpha} = \sum_{\rho\rho'} a_{i\alpha\rho}^\dagger \boldsymbol{\sigma}_{\rho\rho'} a_{i\alpha\rho'}$ and $\boldsymbol{\sigma}$ are the Pauli spin matrices.

As may be observed, the key interactions in this model are: the HOMO-LUMO gap ($\Delta = \epsilon_2 - \epsilon_1$), direct onsite (U) and nearest neighbour (V) MO Coulomb repulsion, spin-exchange (X) and pair

hop (P) between MOs on the same repeat unit, and hopping (t) between neighbouring repeat units. These parameters are the minimum required to model the formation and delocalisation of singlet and triplet excitons along the poly(p -phenylene) backbone.

However, a straightforward derivation of the new Hamiltonian parameters from the atomic Hamiltonian (1) gives results for the excitation energies which deviate substantially from exact Pariser-Parr-Pople model calculations of benzene and biphenyl, as well as to the experimental data on the oligophenylenes [5]. It was shown in [5] that the failure of the 2-MO model is a consequence of the fact that the original HOMO and LUMO single particle basis does not provide an adequate representation for the many body processes of the electronic system. Thus, the orbitals which are assumed to be frozen in the 2-MO model in fact participate dynamically in the many body states. To incorporate this effect one can assume that a two state model, with the relevant many body interactions, is appropriate to describe the low energy physics, but that these interactions are renormalised from their bare Pariser-Parr-Pople values. In this paper we make a thorough investigation of this assumption. We parameterise the two state model by fitting its predictions to the exact Pariser-Parr-Pople model calculations of benzene and biphenyl [15].

2.2 Parameterising the Model

The interactions are parameterised in the following way: First, when the nearest neighbour hybridisation is switched off, the model should predict localised (phenylene) triplet and singlet excitons. As was explained in [5], in contrast to the full Pariser-Parr-Pople calculation of benzene, which predicts a pair of z -polarised and a pair of y -polarised singlet and triplet excitons, the 2-MO model predicts doubly degenerate z -polarised and doubly degenerate y -polarised singlets and triplets. In the 2-MO model the energies of the triplet and singlet are $\sqrt{\Delta^2 + X^2} - P$ and $\sqrt{\Delta^2 + X^2} + P$, respectively. Δ and X (since $P = X$) are determined by fitting these values to the *average* values of the z -polarised triplet and singlet excitons obtained from the full Pariser-Parr-Pople calculation on benzene, which are 4.45 eV and 6.23 eV, respectively [15]. This gives $\Delta = 5.26$ eV and $X = 0.89$ eV. Next, when the

hybridisation is switched on the excitons delocalise and interact. The key low-lying states are the long axis-polarised triplet ($1^3B_u^+$) and singlet ($1^1B_u^-$) states, and the lowest even, *covalent* excitation, the $2^1A_g^+$. Once Δ and X have been fixed, their energies are determined by t , U and V (we assume $|t_{\alpha\beta}| \equiv t$ for all orbitals α, β). We use the exact biphenyl calculations to fit these excitations. To simplify the fitting of these parameters we assume that $V = U/2$, and adjust t and U so that we have an exact fit to the full Pariser-Parr-Pople calculation of the biphenyl $1^1B_u^-$ state and a *minimum* relative error for the $1^3B_u^+$ and $3^1A_g^+$ states. This gives $U = 3.67$ eV, $V = 1.835$ eV, $t = 0.895$ eV, and a relative error for the $1^3B_u^+$ and $3^1A_g^+$ states of -2.2% . We note that since the band width is approximately equal to U , these parameters are in the intermediate coupling regime. This completes the parameterisation of the model.

2.3 Solving the Model

(i) Density matrix renormalisation group solution

The system (3) is a one dimensional quantum lattice model with 16 states per repeat unit. For small lattice sizes, L , it is possible to calculate eigenvalues and eigenstates using exact diagonalisation. However, the largest system which can comfortably be reached by this method is the sexamer ($L = 6$ phenylene units). In order to study larger systems, we turn to the DMRG method [18]. The DMRG is a powerful, robust, portable and highly accurate truncated basis scheme for the solution of low dimensional quantum lattice systems, and is especially well suited to the solution of open linear chains such as (3). We have performed calculations of up to 10 low energy eigenvalues and eigenvectors in the $1^1A_g^+$ and $1^1B_u^-$ symmetry sectors, as well as dipole matrix elements, oscillator strengths and correlation functions for systems of up to 37 repeat units with sufficient accuracy to make comparisons with experiment.

The DMRG is discussed at length in [18] and reviewed in [19] so we restrict our discussion here to features relevant to our implementation of the method for (3). The key features are the form of the *system*, *environment* and *super* blocks, the number m of states retained per block, and the

good quantum numbers used to diagonalise the superblock Hamiltonian and the density matrix. We implement the DMRG for (3) using the *infinite lattice algorithm* [18]. That is, the system and environment blocks are reflections of one another, and are increased by one repeat unit at a time, the initial blocks consisting of a single phenylene unit. The first two superblocks are schematically depicted in Fig. 2. They are comprised of the system and environment blocks abridged by a phenylene repeat unit.

The total charge $\hat{N} = \sum_{i\alpha} n_{i\alpha}$ and the total z spin $\hat{S}_T^z = \frac{1}{2} \sum_{i\alpha} (n_{i\alpha\uparrow} - n_{i\alpha\downarrow})$ are used as good quantum numbers in diagonalising the superblock hamiltonian and the system and environment block hamiltonians and density matrices. In addition, the spatial inversion (\hat{C}_2 : $a_{i\alpha\sigma} \mapsto a_{L-i+1\alpha\sigma}$), particle-hole (\hat{J} : $a_{i1\sigma}^\dagger \mapsto \text{sgn}(\sigma)a_{i2\bar{\sigma}}, a_{i2\sigma}^\dagger \mapsto \text{sgn}(\sigma)a_{i1\bar{\sigma}}$) and spin flip (\hat{P} : $a_{i\alpha\sigma} \mapsto a_{i\alpha\bar{\sigma}}$) symmetry operators can be constructed for the superblock. Their corresponding projection operators can be applied to random superblock states in order to construct trial states of definite symmetries which can be fed into the sparse matrix diagonalisation routine used in the diagonalisation of the superblock hamiltonian. The resulting target states retain these symmetries as long as the iterated trial state is periodically resymmetrised, for example, every 30 or so matrix multiplications. The procedure is verified by calculating the expectation values of \hat{C}_2 , \hat{J} and \hat{P} with respect to the calculated target states. This procedure is numerically stable because the density matrix eigenstates are eigenstates of the block symmetry operators and hence the obtained superblock energy eigenstates are *exact* (to within machine precision) eigenstates of superblock symmetry operators at each iteration. This procedure is checked for each calculated state by determining the expectation values of the symmetry operators, which are found to equal ± 1 to around 12 decimal places.

(ii) Accuracy tests

We verify the validity of the DMRG solution by checking that the results obtained for the trimer and the pentamer agree with exact diagonalisation results. Basis truncation occurs for larger chains, the first being the septamer. This is the largest system that we can treat by exact diagonalisation

(the Hilbert space dimensionality has 11 778 624 basis states). In Table 1 we compare the exact results with two DMRG calculations (with 65 000 and 130 000 states retained) for the energies and exciton sizes of the $1^1B_u^-$ and $2^1A_g^+$ states of this system. It is clearly seen that, despite the fact that the DMRG calculation uses only a fraction of the total number of states (0.55% and 1.10%, respectively), in both cases the results are very close to the exact results, both for the energies and for the exciton sizes.

In order to check the convergence for longer systems we first examine the non-interacting ($U = V = X = P = 0$) case which can easily be diagonalised exactly for any chain length. In the DMRG calculations we retain $m = 230$ states per block. Exact and DMRG results are given in table 2 for the ground and first excited state energies for a number of lattice sizes. We see that the DMRG resolves gaps between these states well and truly above the accuracy required in order to make comparisons with experiments, that is, a few hundreds of an eV. The accuracy is expected to be even better in the interacting case where states are more localised and gaps are widened [18]. That is, the accuracy should increase monotonically as U is increased, up to the atomic limit $t_{\alpha\beta} = 0$ where exact results are trivially recovered by any real space renormalisation group procedure. In Table 3 we monitor the convergence of the optical gap in the interacting case with the truncation parameter m . We again see that the results have converged within errors which are negligible in so far as comparisons with experiment are concerned. Finally, DMRG calculations of the exciton correlation functions of the $1^1B_u^-$ and $2^1A_g^+$ states are checked for systems of up to 21 repeat units by doubling the size of the superbloc Hilbert space. The change in the exciton size is found to be less than 1% for $1^1B_u^-$ and 3% for $2^1A_g^+$ for all the systems studied.

3 The Low Energy Spectra and Exciton Correlation Functions

Table 4 shows the energies of the lowest triplet and singlet B_u excitons as well as the lowest *covalent* even ($^1A_g^+$) excited state. The agreement between the predicted results from the phenomenological model and experiment are good, confirming the validity of our parameterisation. The calculated energies of the lowest excited $^1A_g^+$ and $^1B_u^-$ states as a function of oligomer size N are given in Fig. 3. Also, the charge gap defined as $E_G = E(2N+1) + E(2N-1) - 2E(2N)$, is plotted. Here, $E(2N)$ is the ground state energy of a system with $2N$ electrons. The lowest excited state has $^1B_u^-$ symmetry, its energy being always lower than the charge gap. As the chain length increases, the number of $^1B_u^-$ states below the charge gap also increases, creating an excitonic band in the limit $N \rightarrow \infty$. (There is also a band of $^1A_g^-$ states inter-leaved with the $^1B_u^-$ states.) The energy of the lowest excited $^1A_g^+$ state, $2^1A_g^+$, almost coincides with the charge gap E_G , thus strongly implying that $2^1A_g^+$ is a band threshold state. The energy of the lowest $^1B_u^-$ state above the $2^1A_g^+$, denoted hereafter as $n^1B_u^-$, also tends to E_G as N tends to ∞ . A polynomial fit of the energies as a function of inverse oligomer length indicates that in the limit $N \rightarrow \infty$, the energies of the $2^1A_g^+$ and the $n^1B_u^-$ states, and E_G all tend to a value of 4.04 eV. The energy of $1^1B_u^-$ state tends to 3.30 eV. Thus, the energy results are good evidence that the lowest excited $^1A_g^+$ state is a threshold state dividing the spectrum into bound excitonic states below and unbound band-like states above it.

That the $2^1A_g^+$ state is a band state is confirmed by an examination of the spatial exciton correlation function, as we now demonstrate. In general, any state $|n\rangle$ may be represented as a complete set of excitations from the ground state:

$$|n\rangle = \sum_{ij} C_{ij} S_{ij}^\dagger |1^1A_g^+\rangle + \sum_{ijkl} D_{ijkl} S_{ij}^\dagger S_{kl}^\dagger |1^1A_g^+\rangle + \dots \quad (4)$$

where

$$S_{ij}^\dagger = \frac{1}{\sqrt{2}}(a_{i2\uparrow}^\dagger a_{j1\uparrow} + a_{i2\downarrow}^\dagger a_{j1\downarrow}) \quad (5)$$

is a singlet exciton creation operator, which removes a particle from the orbital $|1\rangle$ on site j and puts

it onto the orbital $|2\rangle$ on site i . Evidently,

$$C_{ij}(|n\rangle) = \langle n | S_{ij}^\dagger | 1^1 A_g^+ \rangle, \quad (6)$$

$$W_1 = \sum_{ij} C_{ij}^2 \quad (7)$$

gives the weight of single particle excitations in the state $|n\rangle$ and

$$P_{ij} = C_{ij}^2 / W_1 \quad (8)$$

is the distribution function for the particle-hole separation. Note that, as discussed in Appendix A, $C_{ij} = +C_{ji}$ for states which are negative under the particle-hole transformation (*i.e.* ‘s’-wave excitons), while $C_{ij} = -C_{ji}$ for states which are positive under the particle-hole transformation (*i.e.* ‘p’-wave excitons).

Using (8), we calculate the spatial extent of a given state, or the particle-hole separation, using the formula:

$$l^2(|n\rangle) = \langle (i-j)^2 \rangle = \sum_{ij} (i-j)^2 P_{ij}. \quad (9)$$

(A similar approach to calculating the average particle-hole separation was used by D. Yaron and R. Silbey in their study of polyacetylene [23].) The results are given in Fig. 4 as a function of oligomer size N . The $1^1 B_u^-$ states belonging to the excitonic band below the charge gap are those with the smallest electron-hole distance. With increasing oligomer size, the particle-hole distance in the $1^1 B_u^-$, as well as in other states in the excitonic band, tends to a limit of approximately one repeat unit. This indicates that these are strongly bound excitons. Conversely, the spatial extent of $2^1 A_g^+$ and $n^1 B_u^-$ states are proportional to the oligomer size, and scale in the same way to N as do the lowest excited (unbound) states (namely, the $1 B_u^-$ and $2 A_g^+$ states) of the *non-interacting* model.

We believe that all these results provide strong evidence that there exists an $1^1 B_u^-$ exciton in PPP, and that the lowest band state has the $1^1 A_g^+$ symmetry. The exciton binding energy for long oligomers tends to $E_G - E_{1^1 B_u^-} = 0.74$ eV.

Finally, in table 5 we show the single particle weight, W_1 (7), for the essential states (as defined in the next section) for a 15 site oligomer. Evidently, these are predominately single particle in

character.

4 Oscillator Strengths and the Linear Susceptibility

As a next step towards the calculation of the NLO properties of PPP, we compute the oscillator strengths of transitions between the essential states. These are, besides the ground state, the $1^1B_u^-$, the $2^1A_g^+$, the $n^1B_u^-$ and also the $1^1A_g^+$ state situated above the $n^1B_u^-$, which we denote as $k^1A_g^+$. This state has already been invoked for explaining the EA spectra of a number of luminescent and non-luminescent polymers by Liess *et al.* [24]. In Fig. 5 we show schematically the most important states for the non-linear optical properties. The results for the corresponding oscillator strengths are given in table 6.

Using the results for the oscillator strengths, the first-order optical absorption is computed. As expected, the dominant peak belongs to the lowest allowed transition, $1^1A_g^+ \rightarrow 1^1B_u^-$, while the band threshold state ($n^1B_u^-$) is represented by a weak feature at 4.3 eV. as shown in Fig. 6 for a 15 site oligomer.

5 Third Order Non-Linear Susceptibilities

The NLO properties of PPP, such as third harmonic generation (THG) and electroabsorption (EA), can be related to the third-order macroscopic susceptibility $\chi^{(3)}$. In Appendix B we show the relationship between the EA-related transmission change, $-\Delta T/T$, and the imaginary part of $\chi^{(3)}(-\omega; \omega, 0, 0)$. The third-order susceptibility $\chi^{(3)}$, in turn, results from the third-order microscopic hyperpolarizability γ_{xxxx} :

$$\chi_{ijkl}^{(3)}(-\omega_\sigma; \omega_1, \omega_2, \omega_3) = \frac{1}{5} f_{xx}^{\omega_\sigma} f_{xx}^{\omega_1} f_{xx}^{\omega_2} f_{xx}^{\omega_3} \gamma_{xxxx}, \quad (10)$$

where $\omega_\sigma = \omega_1 + \omega_2 + \omega_3$ and the factor $\frac{1}{5}$ results from the orientational averaging [25]. The calculation of γ_{xxxx} can be performed using the sum-over-states method (see, e.g., [10]):

$$\gamma_{xxxx}(-\omega_\sigma; \omega_1, \omega_2, \omega_3) = K(-\omega_\sigma; \omega_1, \omega_2, \omega_3)(-\hbar)^{-3}$$

$$\begin{aligned}
I_{1,2,3} \Big(\sum_{A,B,C} & \Big(\frac{\mu_{gA}\mu_{AB}\mu_{BC}\mu_{Cg}}{(\omega_A - \omega_\sigma)(\omega_B - \omega_1 - \omega_2)(\omega_C - \omega_1)} + \frac{\mu_{gA}\mu_{AB}\mu_{BC}\mu_{Cg}}{(\omega_A^* + \omega_3)(\omega_B - \omega_1 - \omega_2)(\omega_C - \omega_1)} + \\
& \frac{\mu_{gA}\mu_{AB}\mu_{BC}\mu_{Cg}}{(\omega_A^* + \omega_1)(\omega_B^* + \omega_1 + \omega_2)(\omega_C - \omega_3)} + \frac{\mu_{gA}\mu_{AB}\mu_{BC}\mu_{Cg}}{(\omega_A^* + \omega_1)(\omega_B^* + \omega_1 + \omega_2)(\omega_C^* + \omega_\sigma)} \Big) - \\
& \sum_{A,C} \Big(\frac{\mu_{gA}\mu_{Ag}\mu_{gC}\mu_{Cg}}{(\omega_A - \omega_\sigma)(\omega_A - \omega_3)(\omega_C - \omega_1)} + \frac{\mu_{gA}\mu_{Ag}\mu_{gC}\mu_{Cg}}{(\omega_A - \omega_3)(\omega_C^* + \omega_2)(\omega_C - \omega_1)} + \\
& \frac{\mu_{gA}\mu_{Ag}\mu_{gC}\mu_{Cg}}{(\omega_A^* + \omega_\sigma)(\omega_A^* + \omega_3)(\omega_C^* + \omega_1)} + \frac{\mu_{gA}\mu_{Ag}\mu_{gC}\mu_{Cg}}{(\omega_A^* + \omega_3)(\omega_C - \omega_2)(\omega_C^* + \omega_1)} \Big) \Big), \quad (11)
\end{aligned}$$

where μ_{ij} is the dipole matrix element for the transition between the states i and j , and $K(-\omega_\sigma; \omega_1, \omega_2, \omega_3)$ is a numerical constant which depends on the values of $\omega_\sigma, \omega_1, \omega_2, \omega_3$ [10]. In particular, for the EA coefficient ($\omega_\sigma = -\omega_1 = -\omega, \omega_2 = \omega_3 = 0$), $K = 3$ and for the THG coefficient ($\omega_\sigma = -3\omega, \omega_1 = \omega_2 = \omega_3 = \omega$), $K = \frac{1}{4}$. $I_{1,2,3}$ denotes the average of all terms generated by permuting ω_1, ω_2 and ω_3 . A finite lifetime of the levels A, B, C is taken into account in order to calculate γ_{xxxx} at the resonance points properly.

The sum in equation (11) is over all states. However, due to the fact that the ground state belongs to the $^1A_g^+$ symmetry sector, the dipole matrix elements are non-zero only for the transitions between $^1A_g^+$ and $^1B_u^-$. Thus, the states A and C in (11) are of $^1B_u^-$ symmetry, while the state B, as well as the ground state, are of $^1A_g^+$ symmetry.

Electroabsorption spectroscopy is used as a tool for investigating the low-lying electronic excitations in polymers (see, e.g., [26, 27, 28]). In [12] it was shown that EA spectrum includes features of two types: First, those similar to the derivative of the first-order optical absorption; they are located at the energies of the $^1B_u^-$ levels. A second type are the peaks at the energies of the $^1A_g^+$ levels, arising from the spatial symmetry breaking in the applied electric field. Recent experimental studies of PPV and PPP EA spectra [29, 24, 4] found both types of features in these systems.

Using the transition matrix elements we calculate the EA spectrum of PPP oligomers using the 10 lowest eigenstates. The results for the 15 site oligomer are shown in Fig. 7. The lowest-energy feature is a derivative-like feature arising from the $^1B_u^-$ level, showing a red shift. Next, the maximum corresponding to the $2^1A_g^+$ state is situated at about 4.3 eV. The second derivative-like feature almost coinciding with the maximum can be related to $n^1B_u^-$ state. Finally, the high energy

at 4.8 eV corresponds to the $k^1A_g^+$ state. For comparison, results of the calculation with the five essential states only are also shown. Evidently, these states describe most of the EA spectrum. The peaks corresponding to the $2^1A_g^+$ and $n^1B_u^-$ states are also identifiable in the EA spectra of Lane *et al.* [4] at approximately 4.1 eV, just below the onset of the 1^1B_{2u} (i.e. short axis-polarised) transition.

Finally, we show the third harmonic generation (THG) spectrum of PPP oligomers. This spectrum is related to the $\chi^{(3)}(-3\omega, \omega, \omega, \omega)$. Mazumdar *et al.* used the THG spectrum in their discussion of the essential states [13]. They argued that there are three main peaks in the THG spectra at $E(1^1B_u^-)/3$, $E(n^1B_u^-)/3$ and $E(m^1A_g^+)/2$, where $m^1A_g^+$ is the $^1A_g^+$ state strongly coupled to the $1^1B_u^-$ exciton. Our calculations (shown in Fig. 8 for a 15 site oligomer) confirm the existence of these peaks (those at 1.15, 1.6, and 2.15 eV, respectively), the $m^1A_g^+$ state being the $2^1A_g^+$ in our model. However, there are additional peaks corresponding to other $^1B_u^-$ and $^1A_g^+$ states (the prominent feature at 3.4 eV corresponds to a one-photon transition to the $1^1B_u^-$ state). The essential states calculation also fails to describe the total THG spectrum (employing 10 states) as well as it does for the EA spectrum.

6 Conclusions

This paper has been devoted to clarifying the nature of the low-lying electronic excitations of PPP. A phenomenological two molecular-orbital (2-MO) model, whose parameters are derived by fitting its predictions to exact Pariser-Parr-Pople model calculations of benzene and biphenyl, was introduced. By solving this model using the DMRG method, it was shown that the lowest excited state is a $^1B_u^-$ exciton, which is situated in the gap between the ground state and the band states. As the oligomer size increases, the number of excitonic levels also increases, thus creating an excitonic band in the limit $N \rightarrow \infty$. The energy of these excitons is consistent with experimental data. The calculated size of these excitons indicates that they are tightly bound, extending over only a few repeat units. The lowest band state is found to be a covalent $2^1A_g^+$ state, whose energy almost coincides for all

the oligomers studied with the charge gap E_G . Lying just above the $2^1A_g^+$ state is a band $^1B_u^-$ state (the $n^1B_u^-$ state). The size of the band states scales linearly with oligomer size. The binding energy of the $^1B_u^-$ exciton is thus determined rigorously as 0.74 eV.

The dipole matrix elements and oscillator strengths for the transitions between the lowest $^1A_g^+$ and $^1B_u^-$ states were calculated and the NLO properties of PPP, such as electroabsorption and third harmonic generation, were investigated. A comparison of the EA spectrum with the experimental data [4] showed that the main features of the experimental spectrum are well described in the 2-MO Hamiltonian. In particular, the derivative-like $^1B_u^-$ feature and the peaks corresponding to the band threshold $2^1A_g^+$ and $n^1B_u^-$ states are reproduced.

Only five states account for most of the calculated electro-absorption. These are the $^1A_g^+$, $^1B_u^-$, $2^1A_g^+$, $n^1B_u^-$ and another band $^1A_g^+$ state, the $k^1A_g^+$, thus confirming the essential states model. An analysis of the particle excitation weight of these states indicates that they are predominately single particle in character.

In conclusion, the parameterised 2-MO model presented here gives a quantitative description of the low lying excitations and the NLO properties of the phenyl based semiconductors. Further improvements of this model will be made by the inclusion of electron-phonon interactions in the phenyl ring and inter-chain interactions.

Acknowledgements

The authors are grateful for valuable discussions with Professor D. Bradley, Dr. S. Martin and Dr. P. Lane from the University of Sheffield and with Dr. Y. Shimoi from the Electrotechnical Laboratory at Tsukuba, Japan. One of the authors (M.Yu.L.) is supported by the EPSRC (U.K.) (grant ref. GR/K86343). R.J.B. acknowledges the support of the Australian Research Council. The calculations were performed on the DEC8400 at the Rutherford Appleton Laboratory and on the SGI Power Challenge facility at the New South Wales Centre for Parallel Computing.

*On leave from Institute of Inorganic Chemistry, 630090 Novosibirsk, Russia

A Particle-hole Symmetry in the Molecular Orbital Basis

In this Appendix we derive the particle-hole inversion operator, \hat{J} , for the molecular orbital (MO) representation, and discuss the particle-hole-symmetry-adapted wavefunctions for a chain. In the atomic orbital (AO) representation the action of the particle-hole inversion operator on the system can be cast as follows:

$$Jc_{i\downarrow}^\dagger = (-1)^i c_{i\uparrow}, \quad (12)$$

$$Jc_{i\uparrow}^\dagger = (-1)^{i+1} c_{i\downarrow}. \quad (13)$$

Using the following relations between the MO and AO creation operators:

$$a_{1\sigma}^\dagger = \frac{1}{\sqrt{12}}(2c_{1\sigma}^\dagger + c_{2\sigma}^\dagger - c_{3\sigma}^\dagger - 2c_{4\sigma}^\dagger - c_{5\sigma}^\dagger + c_{6\sigma}^\dagger), \quad (14)$$

$$a_{2\sigma}^\dagger = \frac{1}{\sqrt{12}}(2c_{1\sigma}^\dagger - c_{2\sigma}^\dagger - c_{3\sigma}^\dagger + 2c_{4\sigma}^\dagger - c_{5\sigma}^\dagger - c_{6\sigma}^\dagger), \quad (15)$$

we deduce the following formulae for the action of the particle-hole inversion on the MOs as:

$$Ja_{1\uparrow}^\dagger = a_{2\downarrow}, Ja_{1\downarrow}^\dagger = -a_{2\uparrow}, \quad (16)$$

$$Ja_{2\uparrow}^\dagger = a_{1\downarrow}, Ja_{2\downarrow}^\dagger = -a_{1\uparrow}. \quad (17)$$

Now let us consider the action of the particle-hole operator within a single exciton basis. Yaron and Silbey have considered the action of \hat{J} on a single exciton basis using periodic boundary conditions [23]. Here, we develop these ideas using the real space MO representation.

Let the ground state be represented by

$$|GS\rangle = \prod_{i=1}^N a_{i1\uparrow}^\dagger a_{i1\downarrow}^\dagger |0\rangle. \quad (18)$$

Then we may create a singlet excitation of spatial extent $\delta = |i - j|$ and localised around the repeat unit $n = (i + j)/2$, as follows:

$$\left| \psi_{n-\delta/2}^{n+\delta/2} \right\rangle = S_{ij}^\dagger |GS\rangle, \quad (19)$$

where

$$S_{ij}^\dagger = \frac{1}{\sqrt{2}}(a_{i2\uparrow}^\dagger a_{j1\uparrow} + a_{i2\downarrow}^\dagger a_{j1\downarrow}). \quad (20)$$

It is straightforward to demonstrate that

$$J \left| \psi_{n-\delta/2}^{n+\delta/2} \right\rangle = -S_{ji}^\dagger |GS\rangle = - \left| \psi_{n+\delta/2}^{n-\delta/2} \right\rangle. \quad (21)$$

Thus, for an exciton localised about repeat unit n we may construct a state with definite particle-hole symmetry as,

$$|\phi_n^\mp\rangle = \sum_{\delta} \left(C_{\delta}^n \left| \psi_{n-\delta/2}^{n+\delta/2} \right\rangle \pm C_{\delta}^n \left| \psi_{n+\delta/2}^{n-\delta/2} \right\rangle \right), \quad (22)$$

where the symmetric ('s'-wave) combination is negative under \hat{J} , while the anti-symmetric ('p'-wave) combination is positive under \hat{J} . It is $C_{\delta}^n = C_{ij}$ which is essentially measured by (6).

A state of definite \hat{C}_2 symmetry may then be constructed as follows:

$$|\psi_j^\mp\rangle = \frac{1}{\sqrt{N+1}} \sum_n |\phi_n^\mp\rangle \sin\left(\frac{n\pi j}{N+1}\right). \quad (23)$$

B Derivation of the Electroabsorption from $\chi^{(3)}$

In this Appendix we present a derivation of the equation relating the electroabsorption signal, $-\Delta T/T$, to the third order nonlinear susceptibility $\chi^{(3)}(-\omega; \omega, 0, 0)$. The polarization induced in the NLO-active crystal subjected to a high-frequency electric field $E(\omega)$ and a low-frequency field F , is given by the following expression:

$$P(\omega) = \chi^{(1)}(\omega, F)E(\omega) = (\chi^{(1)}(\omega) + \chi^{(3)}(-\omega; \omega, 0, 0)F^2)E(\omega) \quad (24)$$

(the absence of the second-order nonlinear susceptibility $\chi^{(2)}$ is provided by the symmetry of the crystal). Hence,

$$\Delta\chi^{(1)}(F) = \chi^{(3)}(-\omega; \omega, 0, 0)F^2, \quad (25)$$

and the change of the dielectric constant ϵ due to the low-frequency field is

$$\Delta\epsilon = 4\pi\Delta\chi^{(1)}(F) = 4\pi\chi^{(3)}(-\omega; \omega, 0, 0)F^2. \quad (26)$$

Using the relation $\epsilon = (n + i\kappa)^2 = n^2 - \kappa^2 + 2in\kappa$, we find

$$\frac{1}{2}\Delta(n^2 - \kappa^2) = n\Delta n - \kappa\Delta\kappa = 2\pi F^2 \text{Re}\chi^{(3)}(-\omega; \omega, 0, 0), \quad (27)$$

$$\Delta(n\kappa) = n\Delta\kappa + \kappa\Delta n = 2\pi F^2 \text{Im}\chi^{(3)}(-\omega; \omega, 0, 0). \quad (28)$$

From these equations the following formula for $\Delta\kappa$ can be deduced:

$$\Delta\kappa = \frac{2\pi F^2}{n^2 + \kappa^2} (n \text{Im}\chi^{(3)}(-\omega; \omega, 0, 0) - \kappa \text{Re}\chi^{(3)}(-\omega; \omega, 0, 0)) \quad (29)$$

The imaginary part of the refractive index, κ , relates to the absorption, α , as follows:

$$\kappa = \frac{c\alpha}{2\omega}, \quad (30)$$

and the change in the normalized transmission $-\Delta T/T$ is

$$-\Delta T/T = \Delta\alpha d = \frac{4\pi\omega F^2 d}{c(n^2 + \kappa^2)} (n \text{Im}\chi^{(3)}(-\omega; \omega, 0, 0) - \kappa \text{Re}\chi^{(3)}(-\omega; \omega, 0, 0)). \quad (31)$$

Using the fact that $\kappa \ll n$, we finally arrive at the relation

$$-\Delta T/T = \frac{4\pi\omega F^2 d}{cn} \text{Im}\chi^{(3)}(-\omega; \omega, 0, 0). \quad (32)$$

References

- [1] J. H. Burroughes, D. D. C. Bradley, A. R. Brown, R. N. Marks, K. Mackay, R. H. Friend, P. L. Burns and A. B. Holmes, *Nature* **347**, 539 (1990).
- [2] G. Grem, G. Leditzky, B. Ullrich and G. Leising, *Adv. Mater.* **4**, 36 (1992).
- [3] C. Ambrosch-Draxl, J. A. Majewski, P. Vogl and G. Leising, *Phys. Rev. B* **51**, 9668 (1995).
- [4] P. A. Lane, M. Liess, Z. V. Vardeny, M. Hamaguchi, M. Ozaki and K. Yoshino, *Synth. Met.* **84** 641 (1997).
- [5] R. J. Bursill, W. Barford and H. Daly *Molecular Orbital Models of Benzene, Biphenyl and the Oligophenylenes*, submitted to *Chemical Physics* (1997).
- [6] W. Barford and R. J. Bursill, *Chem. Phys. Lett.* **268**, 535 (1997).
- [7] J. L. Brédas, *J. Chem. Phys.* **82** (1985) 3808.
- [8] B. Champagne, D. H. Mosley, J. G. Friat and J.M. Andre, *Phys. Rev. B* **54** (1996) 2381.
- [9] Yu. N. Gartstein, M. J. Rice and E. M. Conwell, *Phys. Rev. B* **52** (1995) 1683.
- [10] B. J. Orr and J. F. Ward, *Mol. Phys.* **20**, 513 (1971).
- [11] S. N. Dixit, D. Guo and S. Mazumdar, *Phys. Rev. B* **43**, 6781 (1991).
- [12] D. Guo, PhD thesis, University of Arizona, 1993.
- [13] S. Mazumdar and F. Guo, *J. Chem. Phys.* **100**, 1665 (1994).
- [14] D. Yaron, *Phys. Rev. B* **54**, 4609 (1996).
- [15] W. Barford and R. J. Bursill, *Optimal Parameterisation of the Pariser-Parr-Pople Model for Benzene and Biphenyl*, submitted to *Chem. Phys. Lett.* (1997).
- [16] Z. G. Soos, S. Etemad, D. S. Galvao and S. Ramasesha, *Chem. Phys. Lett.* **194**, 341 (1992).

- [17] M. Chandross, Y. Shimoi and S. Mazumdar, *Synth. Met.* **85**, 1001 (1997).
- [18] S. R. White, *Phys. Rev. Lett.* **69**, 2863 (1992); *Phys. Rev. B* **48**, 10354 (1993).
- [19] G. A. Gehring, R. J. Bursill and T. Xiang, *Acta Physica Polonica* 91 (1997) 105.
- [20] T. G. McLaughlin and L. B. Clark, *Chem. Phys.* 31 (1978) 11.
- [21] L. W. Shacklette, H. Eckhardt, R. R. Chance, G. G. Miller, D. M. Ivory and R. H. Baughman, *J. Chem. Phys.* 73 (1980) 4098.
- [22] B. Tieke, C. Bubek and G. Lieser, *Makroml. Chem. Rapid Comm.* 3 (1982) 261.
- [23] D. Yaron and R. Silbey, *Phys. Rev. B* **45**, 11,655 (1992).
- [24] M. Liess, S. Jeglinski, Z. V. Vardeny, M. Ozaki, K. Yoshino, Y. Ding and T. Barton, to be published.
- [25] D. Neher, W. E. Torruellas, K. B. Rochford, M. B. Marques, R. Zannoni, G. Assanto and G. I. Stegeman, *Synth. Met.* **49-50**, 21 (1992).
- [26] L. Sebastian and G. Weiser, *Chem. Phys.* **61**, 125 (1981).
- [27] L. Sebastian and G. Weiser, *Phys. Rev. Lett.* **46**, 1156 (1981).
- [28] D. Guo, S. Mazumdar, S. N. Dixit, F. Kajzar, F. Jarka, Y. Kawabe and N. Peyghambarian, *Phys. Rev. B* **48**, 1433 (1993).
- [29] S. J. Martin, H. Mellor, D. D. C. Bradley and P. L. Burn, to be published.

Figure Captions

Figure 1 : The structure of the poly(*para*-phenylene) chain.

Figure 2 : Schematic representation of the superblocks used in the first two DMRG steps, showing the form of the system (S) and environment (E) blocks.

Figure 3 : Energies of the lowest excited $^1A_g^+$ and $^1B_u^-$ states relative to the ground state energy, and the charge gap E_G (dashed line) as functions of the oligomer size, N . $^1B_u^-$ (solid squares), $2^1B_u^-$ (solid diamonds), $3^1B_u^-$ (solid triangles), $4^1B_u^-$ (oblique crosses), $n^1B_u^-$ (empty diamonds) and $2^1A_g^+$ (empty squares).

Figure 4 : Mean electron-hole distance for singly-excited low-energy states as a function of oligomer size, N . $^1B_u^-$ (solid squares), $2^1B_u^-$ (solid diamonds), $3^1B_u^-$ (solid triangles), $n^1B_u^-$ (empty diamonds) and $2^1A_g^+$ (empty squares). Results in the absence of electron-electron interactions are shown in dashed lines: $^1B_u^-$ (solid squares) and $2^1A_g^+$ (empty squares). Also shown are dashed lines without symbols corresponding to $N/2$ and $N/4$.

Figure 5 : Essential states for the non-linear properties of the PPP and the most important one-photon transitions between them. The oscillator strengths are shown for a 15 site oligomer.

Figure 6 : Calculated first order optical absorption spectrum for a 15 site oligomer.

Figure 7 : Calculated electroabsorption spectrum for a 15 site oligomer. Solid diamonds: full calculation, empty diamonds: essential states calculation (see text).

Figure 8 : Calculated third harmonic generation spectrum for a 15 site oligomer. Solid diamonds: full calculation, empty diamonds: essential states calculation (see text).

Property	DMRG I	DMRG II	Exact
E_{GS}	-26.821231	-26.821232	-26.821232
E_{1B_u}	-23.239216	-23.239302	-23.239318
E_{2A_g}	-22.254639	-22.254786	-22.254843
$E_{1B_u} - E_{GS}$	3.582015	3.581930	3.581914
$E_{2A_g} - E_{GS}$	4.566592	4.566446	4.566389
R.m.s.($1B_u$)	1.400599	1.398925	1.396940
R.m.s.($2A_g$)	2.660390	2.652987	2.653227

Table 1: Energies of the ground and lowest excited states, as well as exciton sizes of the lowest excited states of a $N = 7$ chain for exact and DMRG calculations (DMRG I: 65,000 states, DMRG II: 130,000 states).

N	E_0 (EXACT)	E_0 (DMRG)	E_1 (EXACT)	E_1 (DMRG)
3	-16.9946597	-16.9946597	-13.9110457	-13.9110457
5	-28.7708529	-28.7708529	-26.3070239	-26.3070239
7	-40.5492152	-40.5492152	-38.3620419	-38.3620023
9	-52.3277963	-52.3277961	-50.2911319	-50.2910587
11	-64.1064055	-64.1064050	-62.1614635	-62.1613673
13	-75.8850187	-75.8850178	-74.0003255	-74.0002074
15	-87.6636326	-87.6636311	-85.8207064	-85.8205619
17	-99.4422467	-99.4422442	-97.6294862	-97.6293092
19	-111.220861	-111.220857	-109.430604	-109.430389

Table 2: Ground and first excited state energies in the non-interacting limit for various oligomer lengths N as calculated exactly and using the DMRG method.

N	$m = 70$	$m = 100$	$m = 130$	$m = 160$	$m = 175$	$m = 210$
7	3.583	3.582	3.582	3.581	3.581	3.581
9	3.480	3.477	3.477	3.477	3.477	3.477
11	3.424	3.420	3.420	3.420	3.420	3.420
13	3.392	3.387	3.386	3.386	3.386	3.386
15	3.373	3.365	3.365	3.365	3.364	3.364
17	3.361	3.351	3.351	3.351	3.350	3.350
19	3.353	3.341	3.341	3.341	3.340	3.340
21	3.348	3.334	3.334	3.334	3.333	3.333

Table 3: Values in eV of the exciton gap, the difference between the ($1^1B_u^-$) and ($1^1A_g^+$) energies, as the truncation parameter m is increased, for a range of oligomer lengths N .

N	$1^1B_u^-$	$2^1A_g^+$	$1^3B_u^+$	Experimental Optical Gap
2	4.80	6.17	3.55	4.80(a)
3	4.28	5.60	3.17	4.5(b)
4	3.98	5.18	2.97	—
5	3.79	4.89	2.85	—
6	3.67	4.70	2.78	3.9(b)
7	3.58	4.57	2.73	—
11	3.42	4.29	2.65	—
13	3.39	4.22	2.63	—
15	3.36	4.18	2.62	—
17	3.35	4.14	2.61	—
19	3.34	4.12	2.60	—
21	3.33	4.11	2.60	—
∞	3.30	4.04	2.60	3.43(b), 3.3(c), 3.5(d), 3.8(e)

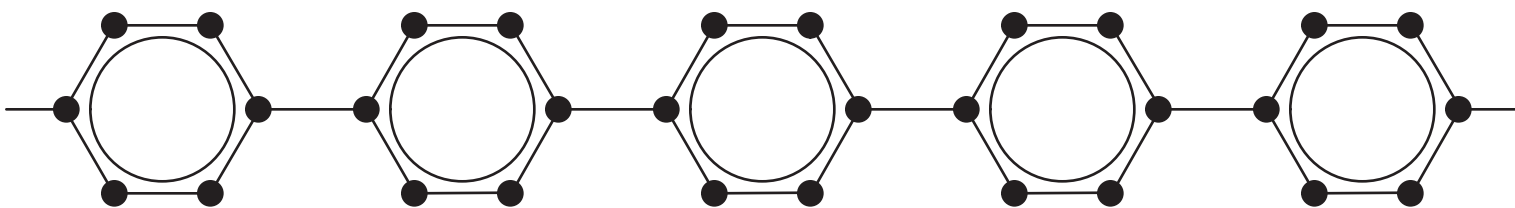
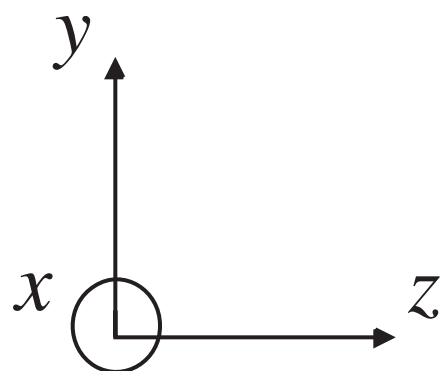
Table 4: Calculated vertical transition energies in eV for oligophenylenes of various lengths N . Note that the $2^1A_g^+$ exciton is the *lowest covalent* A_g singlet excited state. Experimental results from biphenyl crystals (a) [20] and crystalline films (b) [21], (c) [22], (d) [3], (e) [4].

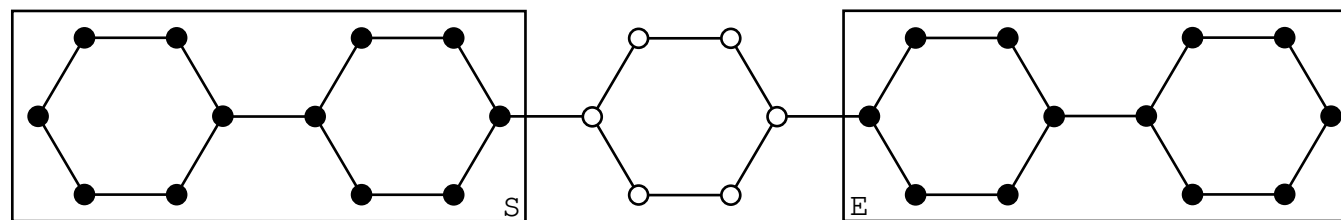
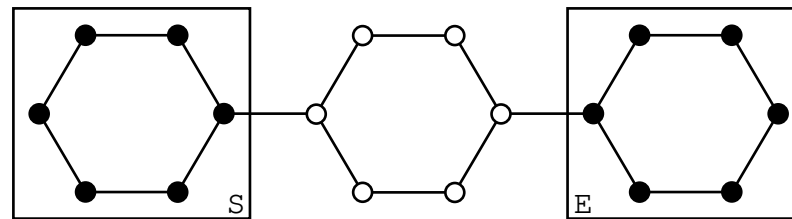
$1^1B_u^-$	$n^1B_u^- (= 4^1B_u^-)$	$m^1A_g^+ (= 2^1A_g^+)$	$k^1A_g^+ (= 4^1A_g^+)$
0.996	0.878	0.794	0.797

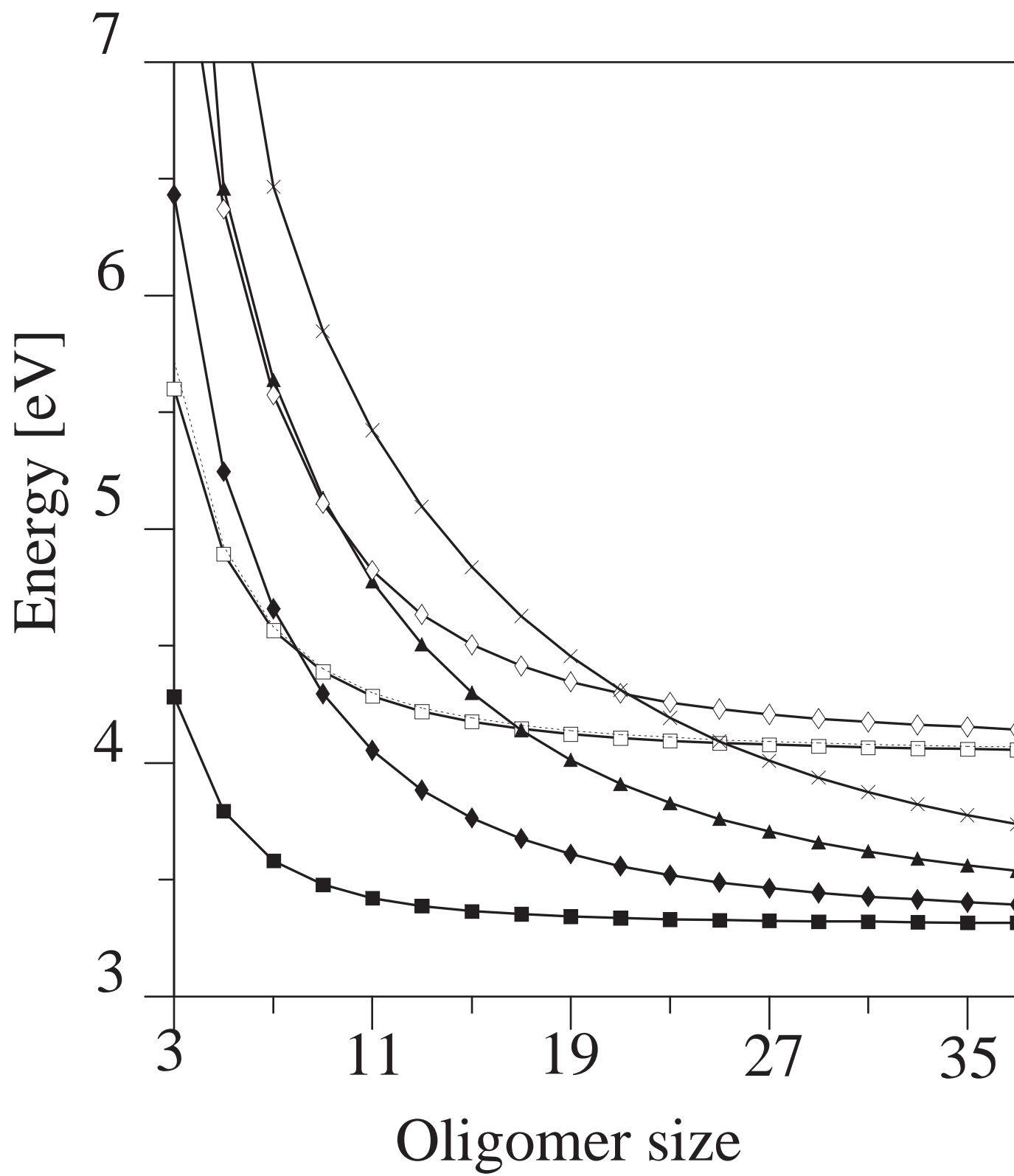
Table 5: The single particle excitation weight, W_1 (7), of the essential states for a 15 site oligomer.

N	$1^1A_g^+ \rightarrow 1^1B_u^-$	$1^1B_u^- \rightarrow 2^1A_g^+$	$2^1A_g^+ \rightarrow n^1B_u^-$	$1^1A_g^+ \rightarrow n^1B_u^-$	$n^1B_u^- \rightarrow k^1A_g^+$
3	21.330 (4.28)	7.091 (1.32)	26.391 (2.23)	0.025 (7.83)	21.202 (1.43)
5	35.858 (3.79)	12.963 (1.10)	48.603 (1.48)	0.314 (6.37)	30.152 (1.04)
7	49.237 (3.58)	21.375 (0.99)	66.291 (1.01)	0.885 (5.58)	40.231 (0.39)
9	62.077 (3.48)	28.833 (0.92)	79.324 (0.72)	1.330 (5.12)	77.925 (0.33)
11	74.603 (3.42)	34.015 (0.87)	87.975 (0.54)	1.664 (4.83)	107.969 (0.29)
13	87.109 (3.39)	37.276 (0.84)	93.555 (0.41)	1.760 (4.64)	124.494 (0.24)
15	99.662 (3.37)	39.144 (0.82)	97.084 (0.33)	1.796 (4.51)	133.758 (0.21)
17	112.411 (3.35)	40.027 (0.80)	99.091 (0.27)	1.727 (4.42)	140.365 (0.18)
19	125.153 (3.34)	40.247 (0.79)	100.176 (0.22)	1.667 (4.36)	144.788 (0.15)
21	138.013 (3.34)	40.142 (0.78)	100.612 (0.19)	1.590 (4.31)	146.118 (0.13)

Table 6: Calculated oscillator strengths for selected transitions in oligophenylenes of various sizes, N . (The corresponding energy differences in eV are shown in brackets.)







Electron-hole distance

10
8
6
4
2
0

7 11 15 19

Oligomer size

